Asian Journal of Chemistry; Vol. 34, No. 4 (2022), 823-833

ASIAN JOURNAL OF CHEMISTRY

https://doi.org/10.14233/ajchem.2022.23588

Electrochemical, Quantum Chemical and Surface Analysis Studies using Novel Schiff Bases for the Inhibition Mild Steel Corrosion in Sulphuric Acid Medium

M. RAGU[1], P. KARUPPASAMY[2], J. THIRUPATHI[3], M. GANESAN[4], T. RAJENDRAN[5] and V.K. SIVASUBRAMANIAN[1,*]

[1]PG and Research Department of Chemistry, Vivekananda College, Tiruvedakam West, Madurai-625234, India
[2]Department of Chemistry, Dayananda Sagar College of Engineering, Bangalore-560078, India
[3]Department of Chemistry, Thiagarajar College, Madurai-625309, India
[4]Department of Chemistry, Sri Vidhya College of Arts and Science, Virudhunagar-626005, India
[5]Department of Chemistry, K.L.N. Arts and Sciences College, Pottapalayam, Sivagangai-630612, India

*Corresponding author: E-mail: sivavk1957@gmail.com; mragu@vivekanandacollege.ac.in

Received: 15 October 2021; *Accepted*: 9 December 2021; *Published online*: 10 March 2022; AJC-20722

The influence of two newly synthesized salophen Schiff bases, namely *N*,*N*′-*bis*(5-nitrosalicylidene)-1,2-phenylenediamine (BNSPD) and *N*,*N*′-*bis*(5-chlorosalicylidene)-*o*-phenylenediamine (BCSPD), for inhibiting mild steel corrosion was investigated using potentiodynamic polarization, weight loss and electrochemical impedance spectroscopy in 0.5 M H_2SO_4 media. The results indicated that the inhibition efficiency of the inhibitors increased and decreased with the increase in the inhibitor concentration and temperature, respectively. Potentiodynamic polarization measurements revealed that the two inhibitors exhibited mixed type. The standard free energy (ΔG°_{ads}) and equilibrium constant of adsorption (K_{ads}) were calculated. Scanning electron microscopy (SEM) and atomic force microscopy (AFM) techniques were used to investigate the surface morphology of the mild steel in the absence and presence of inhibitors. DFT calculations were performed to correlate the molecular structure and quantum chemical parameters with inhibition performance.

Keywords: Corrosion inhibitors, Mild steel, Salophen, Schiff bases, Thermodynamics, Adsorption isotherms.

INTRODUCTION

Metal corrosion has emerged as a problem in different industrial applications, including petroleum production and refining, chemical processing, metal processing and construction [1-4]. Metal corrosion influences the structural insights and performance of metal-based equipment and materials. Material deterioration with corrosion has not only influenced industrial processes but also the economic development [4-6].

However, mild steel is one of the most commonly used metals in residential as well as commercial purposes because of its cost effectiveness, tensile strength and durability. It is remarkable that acidic solutions (especially HCl, H_2SO_4, HNO_3, *etc*.) are widely used in various techniques for cleaning of boilers, aggressive attack of steel materials by corrosive fluids used for acidizing, removal of scale and rust, pickling process, *etc*. [6-8]. Mild steel has easily corroded in acidic nature it induces serious corrosive effect on equipment, tubes and pipelines made of iron and its alloys [9]. Hence, protection of the equipments and vessels made up of mild steel against corrosion is being a major concern in various industries now a day. To control the corrosion of mild steel using different methods such as coating, painting, plating passivation and biofilm formation were studied among them formation protective layer using inhibitor is one of the ways to control corrosion on the mild steel surface [10, 11]. Several studies have been utilized inhibitors such as organic inhibitors (chemical inhibitors), green inhibitors and biological inhibitors to prevent the corrosion of mild steel in the past decade [11-14]. We used Schiff bases as effective corrosion inhibitors in acidic media for mild steel. Sulphuric acid is a highly reactive chemical, which attacks metallic materials utilized for the construction of pipes and storage tanks. Inhibition through Schiff bases is the most efficient approach to protect the metal surface against corrosion in the acidic media [15]. Inhibitor effectiveness depends on the surface covering capabilities and adsorption rates on metals. The main criteria for the

inhibitor adsorption are molecule planarity, π-electron conjugation, and the presence of hetero atoms.

The capacity of inhibitors to adsorb to the metal surface relies on the surface charge and nature of the metal, the electrolyte chemical composition, and electronic characteristics and molecular structure of the inhibitor molecule. Schiff bases, with the general formula of RC=NR′, where R and R′ represent alkyl or aryl groups have the features, when combined with their structure, may lead to the potential inhibition activity. Schiff bases are the products of condensation between amines and aldehydes or ketones. For different metals, some Schiff bases are reported to be effective corrosion inhibitors in the acidic medium [16,17]. The Schiff bases of salicylaldehydes present antibiotic and antimicrobial activities and are reported as the plant growth regulator [18,19]. Schiff bases are used in numerous analytical methods, are highly effective corrosion inhibitors due to their ability to spontaneously form a monolayer on the surface under protection [20,21]. This study investigated the effects of Schiff base inhibitors for the protection of mild steel in 0.5M H_2SO_4. We used two Schiff bases, *N*,*N*′-*bis*(5-nitrosalicylidene)-1,2-pheny-lenediamine (BNSPD) and *N*,*N*′-*bis*(5-chlorosalicylidene)-*o*-phenylenediamine (BCSPD) as inhibitors. Electrochemical impedance spectroscopy and potentiodynamic polarization measurements were used to analyze their inhibition property. The surface morphologies of mild steel samples were studied using atomic force microscopy (AFM), scanning electron microscopy (SEM) and density functional theory (DFT) to confirm the inhibition activity. Langmuir isotherms were analyzed to obtain the adsorption behaviour of the studied compounds.

EXPERIMENTAL

The reactive solution (0.5 M H_2SO_4) was produced by diluting analytical grade 98% H_2SO_4 by using double-distilled water. Before all estimations, mild steel samples (0.38% Si; 0.09% P; 0.01% Al; 0.21% C; 0.05% Mn; 0.05% S and the remainder iron) were polished using different emery papers from grades 80 to 1200 grade. Then, the samples were thoroughly washed with double-distilled water, were degreased with AR-grade ethanol and acetone and finally, were dried at room temperature. Weight loss was measured using mild steel strips with the thickness of 1 cm and dimensions of 4 cm × 1 cm. Strips with an exposed area of 1 cm^2 were utilized in electrochemical experiments. Salicylaldehyde and the substituted salicylaldehydes (5,5′-chloro, 5-nitro) were purchased from Sigma-Aldrich and *o*-phenylenediamine were purchased from Merck (AnalaR grade). The inhibitors were dissolved in acetonitrile in all the experiments. Ethanol was used as a solvent in the synthesis of Schiff bases. These solutions were prepared using AnalaR grade chemicals with conductivity water.

Synthesis of Schiff bases (BCSPD and BNSPD): According to the procedure of Paul *et al.* [22], two salophen Schiff bases*viz*. BCSPD and BNSPD were synthesized by the condensation reaction of an equimolar mixture of *o*-phenylenediamine with two different aldehydes, *p*-chloro salicylaldehyde and *p*-nitro salicylaldehyde using ethanol as solvent [23]. The reaction mixture was refluxed for 5 h and checked for completion using TLC (solvent system ethyl acetate: ethanol, 4:1). The mixture was poured into ice cold water to get a pale yellow solid with a yield of 1.25 g as a crude product, which was then filtered, washed and recrystallized from ethanol (**Scheme-I**). Anal. calcd. (found) % for (BCSPD) $C_{20}H_{14}N_2O_2Cl_2$: C, 62.35 (62.41); H, 3.66 (3.71); N, 7.27 (8.97); O, 8.31 (8.45); and (BNSPD) $C_{20}H_{14}N_4O_6$: C, 59.12 (59.48); H, 3.47 (3.71); N, 13.79 (13.97); O, 23.62 (23.85).

Weight loss measurements: Accurately weighed mild steel test coupons were immersed in 15 mL of 0.5 M H_2SO_4 solution to measure the weight loss in the absence and presence of various concentrations (0.05,0.1,0.2 and 0.3 M) of inhibitors. The immersion time was optimized. This optimized immersion time (1 h) was consistently used to measure weight loss. Then, the test coupons were removed from the electrolyte [24]; they were thoroughly washed with distilled water, dried and weighed. Experiments were conducted in triplicates for all the inhibitor concentrations for reproducibility. The average weight loss was used to calculate the surface coverage (θ), corrosion rate (CR), and inhibition efficiency (IE%). These parameters were determined using the following equations:

$$CR\ (mm\ \ py^{-1}) = \frac{87.6W}{Atd} \quad (1)$$

where W = weight loss, A = area of specimen in cm^2 exposed in acidic solution, t = immersion time in hours, and d = density of mild steel (g cm^{-3}).

$$\theta = \frac{CR_o - CR_i}{CR_o} \quad (2)$$

$$IE\ (\%) = \frac{CR_o - CR_i}{CR_o} \times 100 \quad (3)$$

where CR_o and CR_i are corrosion rate in absence and presence of inhibitors. This experiment was repeated at different temperatures of 300, 310, 320 and 330 K by using water circulated Ultra thermostat to determine the temperature dependence of the inhibition efficiency.

Potentiodynamic polarization measurement: Electrochemical analyses were performed in the conventional three-electrode cylindrical glass cell by using the CH electrochemical analyser model 680 electrochemical workstation at 300 K. The platinum and saturated calomel electrodes were used as the counter and reference electrodes, respectively. Before obtaining the polarisation curves, for 20 min, the solution was deaerated. The working electrode was maintained at the corrosion potential for 10 min to obtain the steady state. The surface of mild steel was exposed to various concentrations (0.05-0.3 M) of BNSPD and BCSPD in an acetonitrile medium with 15 mL of 0.5 M H_2SO_4 at 300-330 K. The inhibition efficiency (IE%) was calculated using eqn. 4:

$$IE\ (\%) = \frac{i^o_{corr} - i_{corr}}{i^o_{corr}} \times 100 \quad (4)$$

here i_{corr} and i^o_{corr} are the values of corrosion current density in the presence and absence of inhibitors, respectively. The

potentiodynamic current-potential curves were measured by automatically varying the electrode potential from -1.5 mV to +1.5 mV against the open-circuit potential with the scan rate of 0.01 mV s^{-1}. This experiment was repeated with the scan rate of 600 mV/min and the corresponding corrosion current (I_{corr}) was measured. Tafel plots were obtained by plotting E *versus* log I. The corrosion current density (I_{corr}), corrosion potential (E_{corr}) and cathodic and anodic slopes (β_c and β_a) were calculated by following a known procedure.

Electrochemical impedance spectroscopy (EIS): Impedance was measured in the frequency of 0.1-10000 Hz at the peak-to-peak amplitude of 20 and 10 mV with the AC signal and open-circuit potential. In the Nyquist representation, the impedance diagrams were plotted. Charge transfer resistance (R_{ct}) was determined by subtracting high-frequency impedance from low-frequency impedance [25]. Eqn. 5 was used to calculate the percentage inhibition efficiency (IE%).

$$IE\ (\%) = \frac{R_{ct(inh)} - R_{ct}}{R_{ct(inh)}} \times 100 \quad (5)$$

where $R_{ct(inh)}$ and R_{ct} are charge transfer resistance in presence and absence of inhibitor, respectively. The values of electrochemical double layer capacitance (C_{dl}) were calculated at the frequency f_{max}, at which the imaginary component of the impedance is maximal ($-Z_i$) in the Nyquist plots by using eqn. 6:

$$C_{dl} = \frac{1}{2\pi f_{max} R_{ct}} \quad (6)$$

Surface characterization: Surface measurements were carried out using JEOL-JSM 5600LVSEM/AFM and images were obtained for mild steel surface after specimen immersion in 0.5 M H_2SO_4 solution in the absence and in the presence of 100 ppm of the inhibitors of BCSPD and BNSPD for 24 h at room temperature [26].

RESULTS AND DISCUSSION

Weight loss measurements: For the mild steel samples, the weight loss caused by corrosion was estimated with different experiments after the addition of various concentrations of BNSPD and BCSPD to the acetonitrile media, with a 24 h immersion time at 300-330 K in 0.5 M H_2SO_4 solution. The experiments were simultaneously performed in triplicate. The average of readings was used. Corrosion rate has been calculated from eqn 1. Inhibition efficiency has also been calculated and the values are given in Table-1. All the two molecules exhibit good corrosion protection of mild steel. The highest value of inhibition efficiency, 94% was shown by BCSPD and 74% by BNSPD in CH_3CN medium at 300 K with 0.3 M concentration of inhibitors. It is pertinent to note two important aspects from the above data. BCSPD has shown higher inhibition efficiency in the order of nineties compare with BNSPD, which has shown the lower inhibition efficiency in the order of seventies. This is attributed to the fact that BNSPD has the presence of powerful electron withdrawing nitro ($-NO_2$) groups in the phenyl moiety. The nitro groups will reduce the electron density in the moiety by that way the metal-inhibitor interaction is lowered which results in the lowering of inhibition efficiency.

Adsorption isotherm: Among the water molecules on a metallic surface (H_2O_{ads}) and organic molecules in aqueous

TABLE-1
INHIBITION EFFICIENCY OBTAINED BY WEIGHT LOSS OF MILD STEEL IN 0.5 M SULPHURIC ACID CONTAINING VARIOUS CONCENTRATIONS OF BCSPD AND BNSPD IN CH_3CN MEDIUM AT DIFFERENT TEMPERATURES

Conc. of inhibitor (M)	BCSPD				BNSPD			
	Weight loss (mg cm^{-2})	CR (mg m^{-2} h^{-1})	IE (%)	Surface coverage (θ)	Weight loss (mg cm^{-2})	CR (mg m^{-2} h^{-1})	IE (%)	Surface coverage (θ)
300 K								
Blank	66.9	0.58	–	–	66.9	0.97	–	–
0.05	31.4	0.35	65	0.65	13.8	0.74	50	0.50
0.1	26.2	0.29	74	0.74	11.3	0.34	61	0.61
0.2	18.4	0.20	85	0.85	8.7	0.15	68	0.68
0.3	10.4	0.11	94	0.94	6.7	0.12	74	0.74
310 K								
Blank	66.9	0.58	–	–	66.9	0.97	–	–
0.05	51.4	0.41	60	0.60	34.5	0.30	47	0.47
0.1	46.9	0.38	68	0.68	22.7	0.25	54	0.54
0.2	33.5	0.26	76	0.76	12.4	0.20	60	0.60
0.3	18.8	0.13	85	0.85	8.9	0.11	69	0.69
320 K								
Blank	66.9	0.58	–	–	66.9	0.97	–	–
0.05	59.0	0.54	52	0.52	47.3	0.59	44	0.44
0.1	52.4	0.44	57	0.57	35.5	0.46	50	0.50
0.2	39.5	0.33	67	0.67	26.9	0.34	57	0.57
0.3	25.7	0.28	75	0.65	20.5	0.17	63	0.63
330 K								
Blank	66.9	0.58	–	–	66.9	0.97	–	–
0.05	57.4	0.48	44	0.44	50.8	0.63	38	0.38
0.1	49.3	0.45	51	0.51	44.5	0.58	46	0.46
0.2	46.9	0.37	58	0.58	38.2	0.47	50	0.50
0.3	37.4	0.29	60	0.60	26.6	0.28	58	0.58

solution (Org_{aq}), the adsorption of organic molecules on the metal/solution interface can be shown as substitution. This process can be given as the following displacement reaction:

$$Org_{(aq)} + nH_2O_{(ads)} \longrightarrow Org_{(ads)} + nH_2O_{(aq)} \quad (7)$$

where n is the number of water molecules eliminated from the metal surface for each inhibitor molecule adsorbed. The n value depends on the cross-sectional area of inhibitor molecules. The inhibitor molecule is adsorbed because of the interaction energy between the metal surface and inhibitor. A correlation between the inhibitor concentration (C_{inh}) and surface coverage (θ) for an electrolyte can be represented using the Langmuir adsorption isotherm (eqn. 8).

$$\frac{C_{inh}}{\theta} = \frac{1}{K_{ads}} + C_{inh} \quad (8)$$

where K_{ads} is the adsorption constant of the equilibrium.

The high K_{ads} value indicates the strong adsorption of the inhibitor on the metal surface. Thus, BNSPD and BCSPD follow the model of Langmuir adsorption, revealing monolayer formation on the metal surface (Fig. 1). For the plot of C_{inh}/θ *versus* C_{inh}, the optimum-fit straight line was obtained with a slope of approximately one. To select the Langmuir isotherm model that well fits the experimental data, the correlation coefficient (r^2) was used. From the intercepts of the straight lines of C_{inh}/θ axis, the values of K_{ads} were calculated and are summarized in Table-2. It is observed for the temperature of 300 K, the value of K_{ads} for BCSPD is 3.87×10^3 which is higher than the K_{ads} of BNSPD (1.98×10^3) at the same temperature. Hence, BCSPD is attributed as a good adsorption inhibitor.

From the values of K_{ads} obtained from Langmuir plots the values of ΔG^o_{ads} have been calculated for BCSPD and BNSPD. The standard free energy of adsorption (ΔG^o_{ads}) and the adsorption constant (K_{ads}) are related by the following equation:

$$\Delta G^o_{ads} = -RT \ln(55.5\ K_{ads}) \quad (9)$$

where R is the universal gas constant, the number 55.5 is the molar concentration of water in solution and T is the absolute temperature. A negative value of ΔG^o_{ads} ensures the spontaneity of the adsorption process and stability of the adsorbed layer on the steel surface [27-29]. Generally, the magnitude of ΔG^o_{ads} around –20 kJ mol^{-1} or less negative is assumed for cases with electrostatic interactions existing between inhibitor and the charged metal surface (*i.e.* physisorption). Those around –30 kJ mol^{-1} indicate chemisorption [30]. The negative ΔH values listed in Table-2 revealed that the adsorption of BCSPD, and BNSPD in CH_3CN on mild steel was observed to be that of an exothermic process. The value is not drastically changed during an increase of temperature, indicating less desorption even at elevated temperatures. The ΔG^o_{ads} values in the present study vary between 28 and 30 kJ mol^{-1} and hence the adsorption process is assumed as chemisorption type [31]. The negative

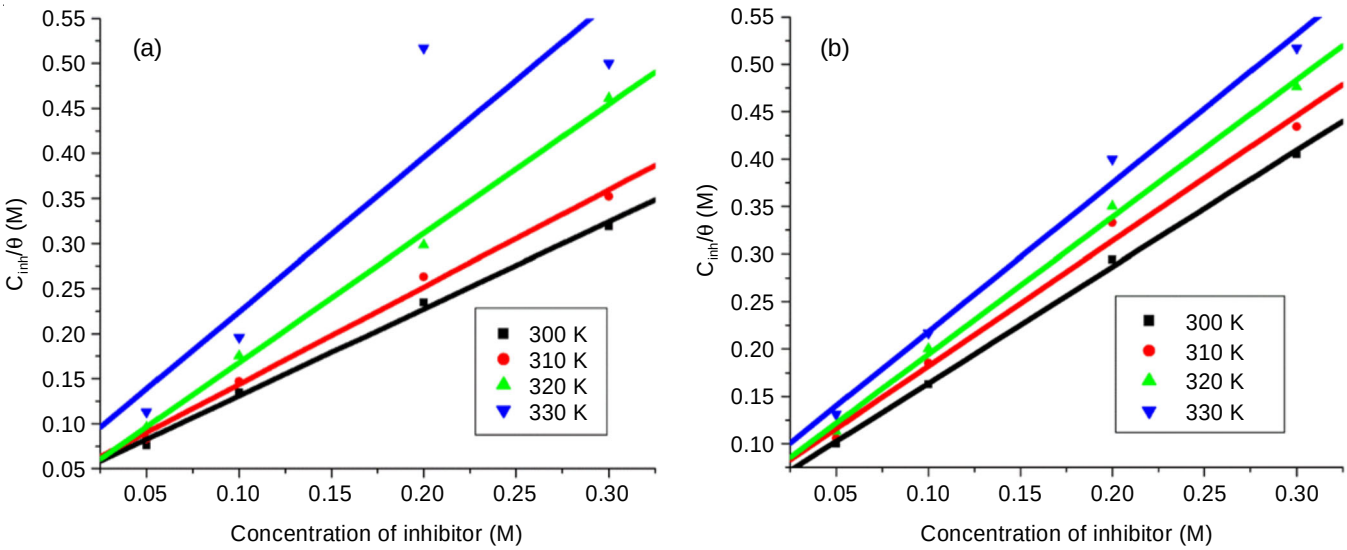

Fig. 1. Langmuir adsorption plots of mild steel in 0.5 M H_2SO_4 at different temperatures for BCSPD (a) and BNSPD (b) in CH_3CN medium

TABLE-2
ESTIMATION OF THE EQUILIBRIUM ADSORPTION CONSTANT (K_{ads}) AND THE FREE ENERGY OF ADSORPTION (ΔG°_{ads}) OF BCSPD AND BNSPD IN CH_3CN MEDIUM ON MILD STEEL SURFACE IMMERSED IN 0.5 M H_2SO_4 SOLUTION. (LANGMUIR ADSORPTION MODEL)

Temp. (K)	BCSPD					BNSPD				
	r^2	K_{ads} (L mol^{-1}) × 10^3	ΔG°_{ads} (kJ mol^{-1})	ΔH_{ads} (kJ mol^{-1})	ΔS_{ads} (kJ mol^{-1})	r^2	K_{ads} (L mol^{-1}) × 10^3	ΔG°_{ads} (kJ mol^{-1})	ΔH_{ads} (kJ mol^{-1})	ΔS_{ads} (kJ mol^{-1})
300	0.98	3.87	-30.62	-32.38	0,05	0.99	1.98	-28.91	-40.09	0.23
310	0.98	2.60	-30.63	-32.38	0.05	0.99	1.76	-29.61	-40.09	0.22
320	0.98	1.51	-30.15	-32.38	0.06	0.99	0.82	-28.54	-40.09	0.21
330	0.98	1.24	-30.56	-32.38	0.05	0.99	0.50	-28.07	-40.09	0.20

value of ΔG^{o}_{ads} indicates the stability of the adsorbed layer on the steel surface and spontaneity of the adsorption process. The other thermodynamic functions can also be calculated from the following equation:

$$\Delta G^{o}_{ads} = \Delta H_{ads} - T\Delta S_{ads} \quad (10)$$

where ΔH^{o}_{ads} and ΔS^{o}_{ads} are the enthalpy and entropy of adsorption, respectively.

Electrochemical measurements

Tafel polarization studies: Fig. 2 show the effect of two inhibitors (BNSPD and BCSPD) on the potentiodynamic polarization behaviour of mild steel in the CH_3CN medium and 0.5 M H_2SO_4 acid solution at 300 K. Table-3 presents the inhibition efficiency values (η%) and corrosion parameters, including cathodic and anodic Tafel slopes (β_c and β_a), corrosion potential (E_{corr}) and corrosion current density (I_{corr}), acquired by extrapolating the Tafel lines. The polarization curves indicated that the rates of both the anodic and cathodic reactions decreased with increase in the inhibitor concentration and decrease in current densities. With inhibitor addition, cathodic hydrogen evolution and anodic dissolution retard. On the metal surface, the electrochemical processes are related to inhibitor adsorption [32-36]. Adsorption depends on the inhibitor's chemical structure. Some difference can be observed in the values of E_{corr} between the inhibitor containing and blank systems. However, for inhibitor containing systems, E_{corr} values essentially shift towards the anodic and cathodic regions in relation to that in the blank systems (Fig. 2). The inhibitor can be considered as only cathodic or anodic type when E_{corr} displacement is > 85 mV [37-39]. The shift in E_{corr} for the presented salophen Schiff base is not that large; thus, they are considered mixed type inhibitors. The gradual inhibitor concentration increase causes corrosion current densities to decrease. A marked decrease is observed in corrosion current densities when the inhibitor concentration increases. Therefore, in the presence of inhibitors, the decrease in current density indicates that corrosion proceeds considerably slower in the inhibited medium than the uninhibited medium. The increase in inhibitor concentrations leads to the increase in the surface coverage values, which consequently causes the decrease in corrosion current densities (Table-3). The maximum inhibition efficiencies of 74% and 93% were obtained for BNSPD and BCSPD, respectively, at 0.3 M in the acetonitrile medium. The increase and decrease in the inhibition efficiency and corrosion current densities, respectively, observed with the increase in the inhibitor concentration indicate that additional inhibitor molecules adsorbed on the metal surface, thereby providing a wider surface coverage [40]. These compounds served as excellent adsorption inhibitors.

Electrochemical impedance spectroscopy (EIS): The corrosion behaviours of mild steel comprising various salophen

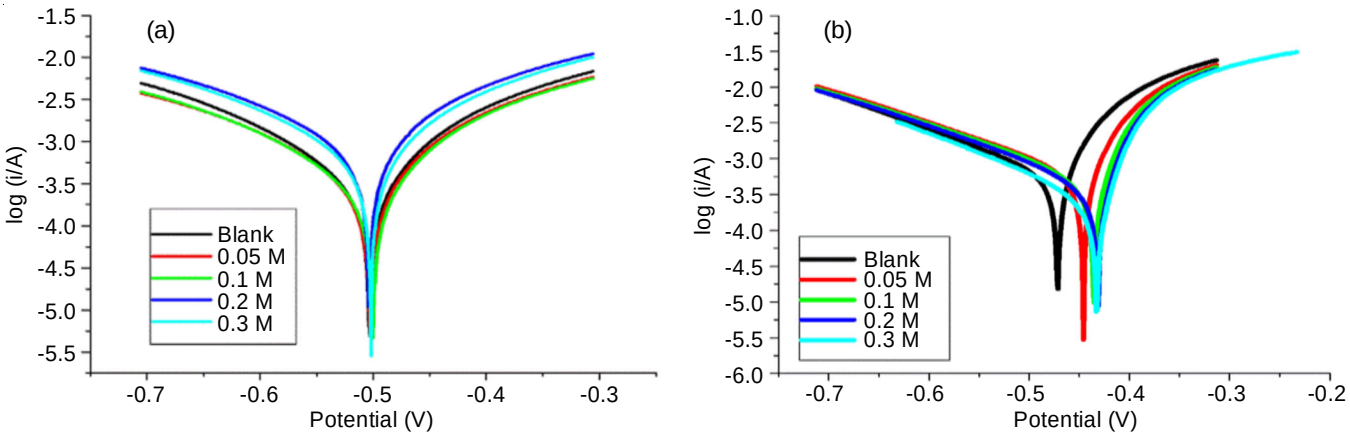

Fig. 2. Tafel polarization curves of mild steel in 0.5 M H_2SO_4 at 300 K in the presence of BCSPD (a) and BNSPD (b) in CH_3CN medium at different concentrations

TABLE-3
INHIBITION EFFICIENCY OBTAINED BY TAFEL POLARIZATION OF MILD STEEL IN 0.5 M H_2SO_4 CONTAINING VARIOUS CONCENTRATIONS OF BCSPD, AND BNSPD IN CH_3CN MEDIUM AT 300 K

Inhibitors concentration (M by weight)	E_{Corr} (mV/SCE)	I_{Corr} (μA cm^2)	β_C (mv/dec)	β_a (mv/dec)	IE (%)	Surface coverage (θ)
BCSPD Blank	-501	-960	246	204	–	–
0.05	-482	-360	175	158	70	0.70
0.1	-441	-337	138	123	83	0.83
0.2	-431	-286	109	104	89	0.89
0.3	-424	-225	064	67	93	0.93
BNSPD Blank	-501	-960	246	204	–	–
0.05	-445	-489	173	165	55	0.55
0.1	-435	-470	153	137	60	0.60
0.2	-425	-435	136	110	69	0.69
0.3	-420	-418	107	75	74	0.74

inhibitor concentrations were investigated in 0.5 M H_2SO_4 through electrochemical impedance spectroscopy (EIS). Fig. 3 presents the Nyquist plots comprising capacitive loops; these plots revealed that capacitive loops are imperfect semi-circles possibly resulting from frequency dispersion, inhomogeneity, and roughness of the metal surface, grain boundaries, impurities and surface active site distribution. Thus, in the circuit, the constant phase element (CPE) was introduced to acquire a highly accurate fit [41-43]. Table-4 presents the influence of inhibitor concentrations on mild steel corrosion in 0.5 M H_2SO_4 at 300 K. These plots present a depressed semi-circle. The semi-circle size increases with the increase in the inhibitor concentration from 0.05 to 0.3 M. The electrochemical corrosion kinetic parameters such as charge transfer resistance (R_{ct}), double layer capacitance (C_{dl}) are calculated from the Nyquist plots and the obtained data are presented Table-4.

The maximum inhibition efficiency was achieved at 0.3 M inhibitor concentration for the two inhibitors. The fact that the charge transfer resistance value increased with increasing inhibitor concentration infers that the considerable surface coverage area is present in the inhibitor and also strongly binds to the surface of mild steel [44-47]. The obtained results are comparable with the reported heterocyclic systems, because all the inhibitors used in this present system have the hetero atoms in the cyclic ring.

The presence of the single semicircle was attributed to single charge transfer that occurred during metal dissolution. For the frequency independent phase shift between the current response and applied AC potential, CPE can be employed, which is defined in impedance presented in eqn. 6. The n value (changing between 0.7 and 0.95) indicates the deviation from the ideal behaviour (where n = 1). The ideal behaviour is used as the measure of surface in-homogeneity. The Nyquist plots can be described on the basis of an equivalent circuit comprising parallel-connected charge transfer resistance (R_{ct}) to CPE in series with solution resistance.

Table-4 shows that there is a significant increase in the values of R_{ct} with increase in the concentration of the inhibitors and corresponding decrease in C_{dl} values. The increase in charge transfer (R_{ct}) values infer the formation of protective surface film on the metal surface. However, the decrease in C_{dl} values indicate, a decrease in local dielectric constant and an increase in the thickness of protective layer at the metal surface which protects the metal from corrosion. This particular inference of decrease in C_{dl} values and increase R_{ct} values with change in concentration of inhibitors show that the inhibitors retard corrosion by the phenomenon of adsorption. The phase angle shifted with the increase in the inhibitor concentration. The shift may result from protective film formation on the steel surface, which leads to change in the interfacial structure of the electrode [48]. At high concentration, the larger is the surface areas occupied by Schiff bases, the higher is the phase shift. The trend of the current passing through the capacitor can be attributed to the increase in the impedance value with the

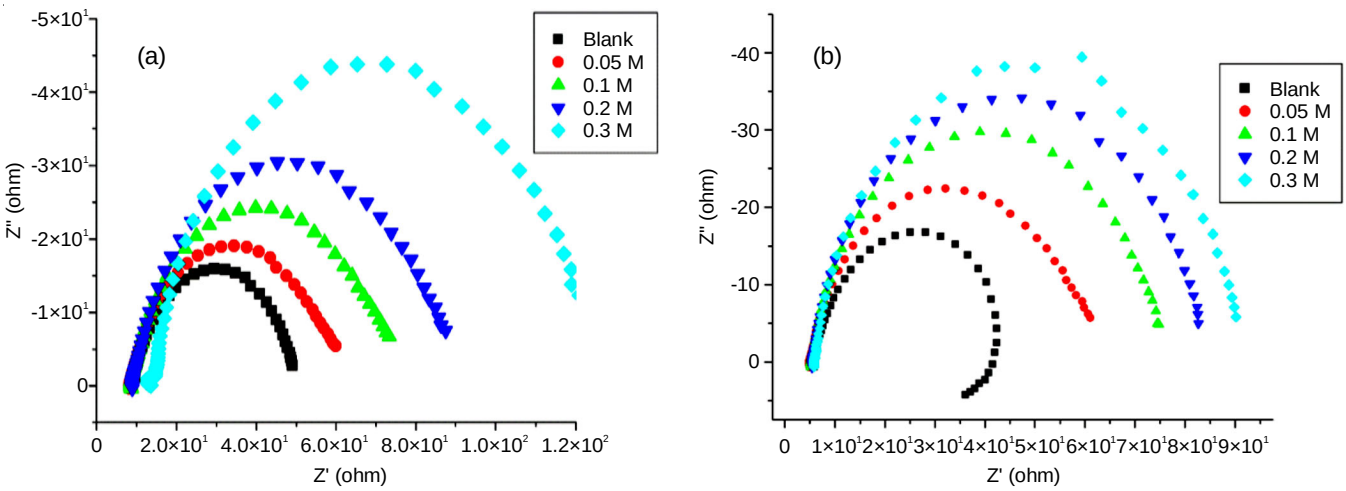

Fig. 3. Nyquist plots of EIS measurements of mild steel in 0.5 M H_2SO_4 at 300 K in the presence of inhibitior [BCSPD (a) and BNSPD (b)] in CH_3CN medium at different concentrations

TABLE-4
INHIBITION EFFICIENCY OBTAINED BY EIS MEASUREMENTS OF MILD STEEL IN 0.5 M H_2SO_4 CONTAINING VARIOUS CONCENTRATIONS OF BCSPD AND BNSPD IN CH_3CN MEDIUM AT 300 K

Inhibitors concentration (M by weight)	BCSPD				BNSPD			
	R_{ct} (Ω cm^2)	C_{dl} (μF cm^2)	IE (%)	Surface coverage (θ)	R_{ct} (Ω cm^2)	C_{dl} (μF cm^2)	IE (%)	Surface coverage (θ)
Blank	25	40	–	–	25	40	–	–
0.05	40	76	72	0.72	45	67	44	0.44
0.1	55	65	84	0.84	97	58	74	0.74
0.2	70	51	90	0.90	140	41	82	0.82
0.3	110	39	95	0.95	240	34	89	0.89

increase in the inhibitor concentration. The EIS results are in a strong agreement with the polarization measurement findings. EIS studies supported the increase in the inhibition efficiency of BNSPD and BCSPD with the increase in their concentration. However, BCSPD exhibited higher inhibition efficiency than BNSPD at similar concentrations.

Mechanism of inhibition: In the acetonitrile medium, the inhibition efficiency of BNSPD and BCSPD against mild steel corrosion in 0.5 M H_2SO_4 was explained according to molecular size, the number of adsorption sites, and mode of interactions with the metal surface. The two inhibitors comprise an imide bond, nitrogen atoms in the ring and π-electrons that serve as adsorption centres. Thus, the inhibitor chemisorbs onto the mild steel surface through coordinate bonding with these electrons. Nitrogen atoms can easily be protonated and the protonated species binds physically to the positively charged surface of mild steel through the negatively charge sulphate ion (SO_4^{2-}). In acetonitrile medium, the chlorine atoms of BCSPD have a lone electron pair, which is donated to the *d*-orbital of Fe atom [49]. Therefore, the existence of chlorine atom leads to the strong BCSPD inhibition efficiency in the acetonitrile medium. The decrease in the inhibition efficiency of BNSPD in CH_3CN medium was caused by the existence of the strongest deactivating group, that is, the nitro group. On benzene ring, the nitro group reduces the electron density; hence, the inhibition efficiency declines.

The phenomenon of adsorption plays an important role in the inhibitive action of inhibitors on the corrosion of metals in acid media. Indeed, the inhibitor protects the metal from corrosion by forming a protective layer on the metal surface. Higher the stability of the protective layer higher will be its inhibitive action. The protective action of the inhibitor is attributed to various reasons such as (i) interaction of unshared electron pair of inhibitor molecule with metal, (ii) interaction of π-electron cloud present in the multiple bonds and aromatic system of inhibitors with metal, and (iii) charged inhibitor molecules in acid media will have electrostatic interaction with metal surface.

In present work, the thermodynamic parameters particularly the ΔG values infer the mode of adsorption of inhibitor on the metal surface. The ΔG values are negative and hence the adsorption process is spontaneous. The magnitude of the ΔG values indicate that adsorption is chemisorption in nature. In this chemisorptive phenomenon, the lone pair of electrons present in the nitrogen atom of the inhibitor will form a coordinate bond with the vacant *d*-orbital of the metal. Further the stainless steel surface in acid media is positively charged. In the positively charged metal surface the negatively charged sulfate (SO_4^{2-}) ions are adsorbed making the surface of the metal negatively charged. The inhibitor molecules having the higher electron cloud is highly susceptible for protonation in acid medium. The protonated inhibitor molecules will readily interact with negatively charged metal surface by electrostatic interaction leading to the better and compact adsorption of inhibitor molecules. The increase in the efficiency of inhibition with increasing concentration of inhibitor makes the adsorptive layer thick, which facilitate better inhibition and protection of metal from corrosive media [50].

The formation of coordinate bond between the metal and inhibitor is explained as follows. In the aqueous acidic medium, the metal is initially oxidized to Fe^{2+} ions and further Fe^{2+} ions are oxidized to Fe^{3+} ions. The formation of these ion is not favourable since they are not passive. However, these ions will form a coordinate bond with the nitrogen present in the inhibitor which leads to complex formation. The complex formed will act as good shield to the metal surface that will protect the metal from corrosion.

Scanning electron microscopy (SEM): The SEM analysis was carried out in order to verify the adsorption of inhibitor on the mild steel surface. The SEM micrographs obtained for the mild steel surface in the absence and presence of optimum concentration of 0.1 mM inhibitor BCSPD and BNSPD in the acetonitrile medium in 0.5 M H_2SO_4 after 4 h of immersion time at 30 ºC are shown in Fig. 4. The mild steel surface in the absence of inhibitor was highly corroded due to aggressive nature of sulphuric acid 0.5 M. The SEM image of mild steel surface in the presence of BCSPD in acetonitrile medium is smooth, which shows a high degree of protection for the mild steel surface by the inhibitor BCSPD in acetonitrile medium . The SEM image of mild steel surface in the presence of BNSPD in acetonitrile medium is good, however, the surface is consisting of some pits.

Atomic force microscopy (AFM) studies: AFM is a promising method used to analyze the surface morphology on

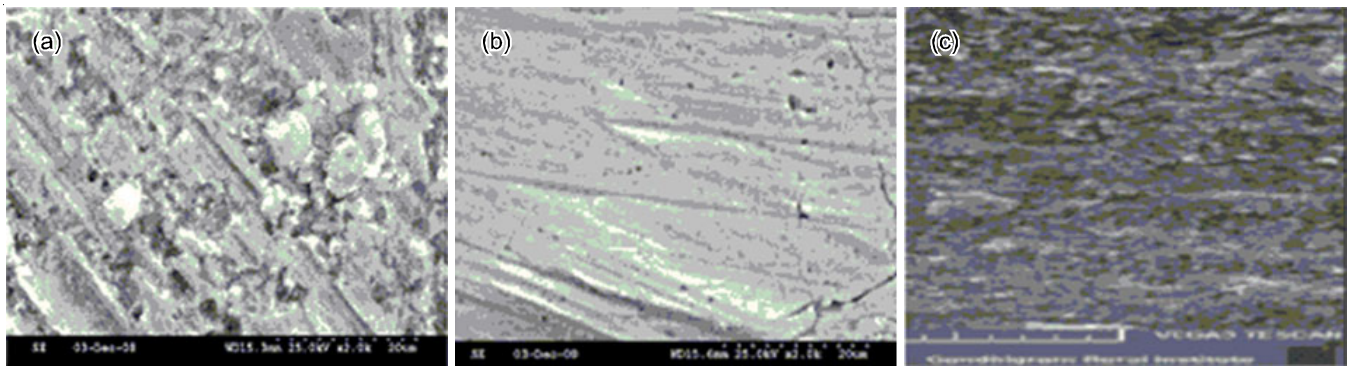

Fig. 4. Scanning electron micrographs of mild steel surface (a) without inhibitor (b) with inhibitor BCSPD (0.1 mM) in 0.5 M H_2SO_4 in CH_3CN medium (c) with inhibitor BNSPD (0.1 mM) in 0.5 M H_2SO_4 in CH_3CN medium

nano-scale to microscale and has emerged as an alternative to investigate the effect of inhibitor molecules for controlling corrosion at the metal/solution interface. The image analysis allowed surface roughness quantification for the area of 12 × 12 μm^2. Atomic force microscopy was employed to measure the three dimensional topography. The three-dimensional AFM images are shown in Fig. 5. As can be seen from the figure, there was much less damage on the surface of mild steel surface dipped in 0.5 M H_2SO_4 solution in the presence of the inhibitors BCSPD and BNSPD in acetonitrile medium as compared to the mild steel in 0.5 M H_2SO_4 in absence of inhibitors, which is attributed to the formation of a protective layer by inhibitors. Hence, the inhibitors hinder the dissolution of iron and there by decrease the rate of corrosion of mild steel in 0.5 M H_2SO_4.

Computational study: Molecular structures of the inhibitors play an important role in the process of corrosion inhibition of metals in severe acidic medium. Organic molecules satisfy the necessary conditions to act as good inhibitors. In choosing organic molecules as inhibitors it is pertinent to keep the following points in mind. The chosen organic molecules should be perfectly aromatic compounds with extensive conjugation, presense of oxygen and nirtogen atoms having lone pair of elcetrons which are free to move to the unoccupied electronic levels of metal atom. Complete planarity of the organic molecule is highly preferable to have better adsorption on the metal surface and to act as a barrier in the metal/solution interface to control corrosion. Above all the synthesis and characterization of inhibitor molecules must be easy and they should be eco-friendly.

Extensive experimental methods such as weight loss, potentiodynamic polarization, electrochemical imperdance spectroscopy (EIS), have been carried out to assess the efficiency of the inhibitor. These experimental techniques vividly give the inhibition efficiency and other adsorption characteristics of inhibitors BCSPD and BNSPD. The quantum chemical calculations were carried out for the inhibitors BCSPD and BNSPD to understand the impact of molecular structure on the inhibition efficiency using density functional theory (DFT) method. The quantum chemical calculations were performed using Gaussian 16 (Revision A.03) Suite of programs [51]. The inhibitors were optimized in gas phase with Becke's three parameter and Lee-Yang-Parr's correlation hybrid (B3LYP) functional in conjugation with Pople's 6-31G (d) basis set to calculate the physical properties of the inhibitors [52,53]. The vibrational frequency analysis was performed at the same level of theory to confirm the minimum energy value on the potential energy surface.The calculated quantum chemical parameters such as the energy of highest occupied molecular orbital (E_{HOMO}) and lowest unoccupied molecular orbital (E_{LUMO}), energy gap (ΔE), absolute electronegativity (χ), dipole moment (μ), global hardness (η), softness (σ), electronegativity (ω), nucleophilicity (ε) and fraction of electrons transferred from the inhibitor molecule to the metal surface (ΔN) are summarized in Table-5.

TABLE-5
CALCULATED QUANTUM CHEMICAL PARAMETERS FOR THE INHIBITORS BCSPD AND BNSPD

Quantum chemical parameters	Schiff base inhibitors	
	BCSPD	BNSPD
E_{HOMO} (eV)	-5.92	-6.51
E_{LUMO} (eV)	-2.11	-2.53
ΔE (eV)	3.80	3.97
χ (eV)	4.01	4.52
μ (D)	3.394	5.732
η (eV)	1.90	1.99
σ (eV)	0.53	0.50
ω (eV)	4.24	5.14
ε (eV)	0.24	0.19
ΔN (e)	0.785	0.624

The optimized geometrical structures of BCSPD and BNSPD are given in Fig. 6. The HOMO and LUMO orbitals of the inhibitor BCSPD and BNSPD are given Figs. 7 and 8 respectively. In the molecule, there are regions which have rich electron density that constitute the HOMO of the molecule.

These regions are the centre for electrophilic attack. In the inhibitor BCSPD and BNSPD molecule the nitrogen atom of the imine group, oxygen atom of the hydroxyl groups and the benzene rings constitute the areas of bounteous electron density. These parts will readily interact with the atoms in the surface of the metal. However, the LUMO of the inhibitors is the centre to accept electrons of the metal surface to form anti-bonding molecular orbitals. It is observed that the LUMO of

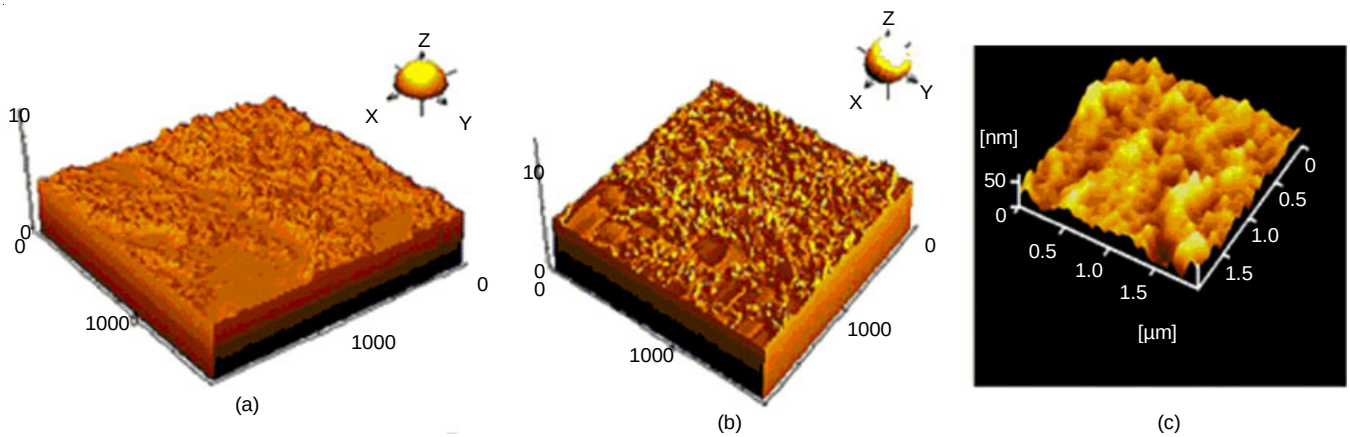

Fig. 5. Atomic force micrographic image of of mild steel surface in 0.5 M H_2SO_4 (a) without inhibitor (b) with inhibitor BCSPD (0.1 mM) in CH_3CN medium, (c) with inhibitor BNSPD (0.1 mM) in CH_3CN medium

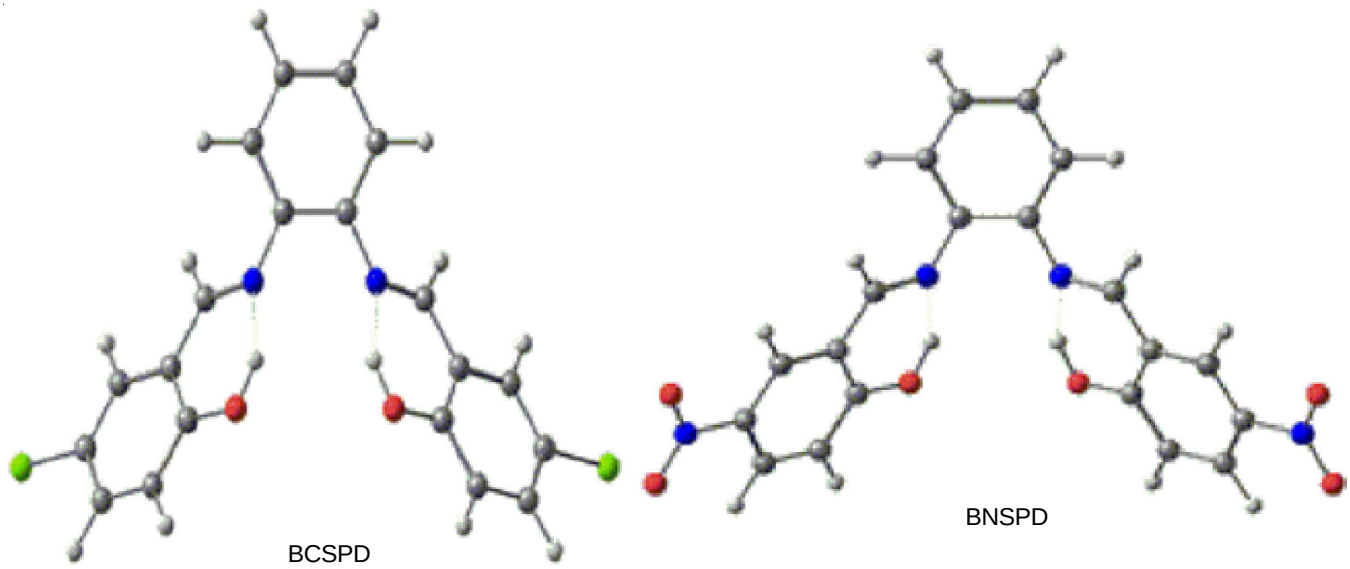

Fig. 6. Opimized geometrical structures of BCSPD and BNSPD in CH_3CN medium

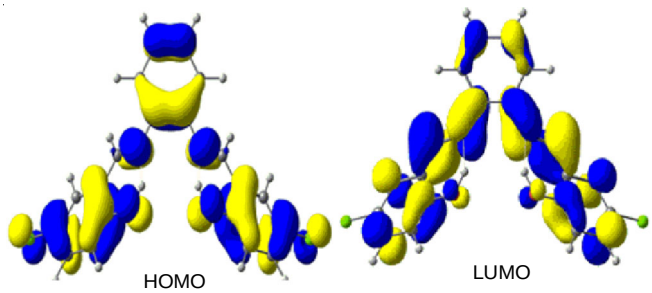

Fig. 7. HOMO and LUMO orbitals of BCSPD

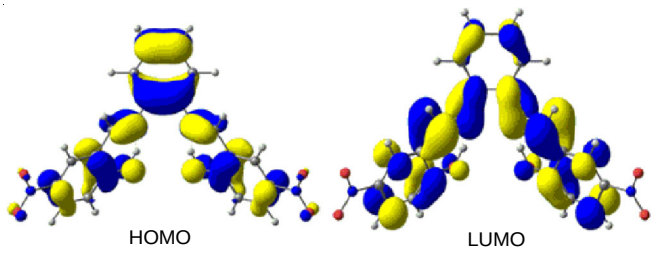

Fig. 8. HOMO and LUMO orbitals of BNSPD

BCSPD is mainly confined on the electronegative chlorine atom and part of pi-bonds of aromatic rings. These regions are capable of accepting electrons from metal to form antibonding orbitals to form backbond. The values of (E_{HOMO}) of the inhib-itors BCSPD and BNSPD are higher than the (E_{LUMO}) values of the inhibitors, respectively (Table-5). These values show that the electrons can be easily donated from the HOMO orbitals to the appropriate orbitals of receiving centres namely the metal orbitals.

The energy difference between HOMO and LUMO orbitals $E_{LUMO} - E_{HOMO}$ (ΔE) is an important parameter which decides the efficiency of the inhibitor. High values of inhibition efficiency is correlated with the lower values of ΔE. This is attributed to the fact of lowest excitation energy that facilitates the removal of electrons from the last filled orbital that makes better adsorption of the inhibitors [54-56]. For the two inhibitors BCSPD and BNSPD, the ΔE of the former is 3.80 eV where as of the latter is 3.97 eV, which shows BCSPD is a better inhibitor than BCSPD. Other parameters given in Table-5 also support the better efficiency of BCSPD than BNSPD.

For a molecule to act as a good inhibitor,the parameter (ΔN), number of electrons transferred from the inhibitor molecule to the metal centre should be high. It is pertinent to note that the value of ΔN for BCSPD is 0.785 and for BNSPD is 0.624. Hence BCSPD will act as a good inhibitor .Another factor which decides the supremacy of an inhibitor is the value of dipolemoment (μ). Dipole moment is a physical parameter, which tells about the disrtibution of charges in the molecule based on the elctronegativity difference of atoms involved in the bond formation. There is a difference of opinion among the researchers in using the dipole mement as the deciding factor to chose a molecule to act as an inhibitor. It is observed that a molecule having lower value of dipolemoment can act as a good inhibitor. This idea prompts to say that a polar molecule which possess lower dipolemoment will have better adsorption on the metal surface leading to higher inhibitor efficiency. In present system, molecule BCSPD is having the dipole moment of 3.394, which is lower than the dipole moment of BNSPD having value as 5.732 D [57].

The DFT data also projects the values of hardness and softness.The value of global hardness (η) for BCSPD is 1.90, which is smaller than the value for BNSPD (1.99). Usually the lower values of η is a good indicator to support supremacy of the inhibitor [58]. The calculated quantum chemical parameters are in agreement with the experimental values obtained for the inhibitors BCSPD and BNSPD to contol corrosion in the present investigation. Hence, the computational studies also indicate the supremacy of the inhibitor BCSPD to protect the mild steel in the corrosion process with sulphuric acid medium in comparison with BNSPD.

Conclusion

Two novel salophen Schiff bases, *viz. N,N′-bis*(5-nitrosalicylidene)-1,2-phenylenediamine (BNSPD) and *N,N′-bis*(5-

chlorosalicylidene)-*o*-phenylenediamine (BCSPD) as corrosion inhibitors, exhibited considerably a high inhibition efficiency in 0.5 M H_2SO_4 medium. The inhibition efficiency obtained through potentiodynamic polarization, weight loss, electrochemical impedance spectroscopy, AFM, SEM and computational methods showed that in the acetonitrile medium, both BNSPD and BCSPD Schiff bases act as good inhibitors. However, the inhibition efficiency order is BCSPD > BNSPD. The inhibition efficiency increases and decreases with the increase in the concentration and temperature, respectively. The evaluated adsorption isotherm and thermodynamic parameters revealed that the adsorption involves chemisorption and exhibits the Langmuir type. Polarization studies indicated that the inhibitor affects the cathodic and anodic reactions. Impedance studies revealed that in the presence of inhibitor, the higher charge transfer resistance results in higher inhibition efficiency. Morphological studies confirmed that inhibitors control corrosion by forming protective layers on the mild steel surface. The computational study complements the effectiveness of two molecules as inhibitors in the corrosion of mild steel with H_2SO_4 medium. However, the better inhibitive property of BCSPD molecule on comparison with BNSPD molecule is also supported by computational data.

ACKNOWLEDGEMENTS

The author thanks the Management, Principal and Head of the Department of Chemistry, Vivekananda College, Tiruvedakam West, India for providing the research facilities.

CONFLICT OF INTEREST

The authors declare that there is no conflict of interests regarding the publication of this article.

REFERENCES

1. A. Dehghani, G. Bahlakeh, B. Ramezanzadeh and M. Ramezanzadeh, *Constr. Build. Mater.*, **245**, 118464 (2020); https://doi.org/10.1016/j.conbuildmat.2020.118464
2. P.S. Neriyana and V.D.P. Alva, *Chem. Africa*, **3**, 1087 (2020); https://doi.org/10.1007/s42250-020-00190-z
3. K. Muthukumarasamy, S. Pitchai, K. Devarayan and L. Nallathambi, *Mater. Today Proc.*, **33**, 2214 (2020); https://doi.org/10.1016/j.matpr.2020.06.533
4. H. Lgaz, S.K. Saha, A. Chaouiki, K.S. Bhat, R. Salghi, Shubhalaxmi, P. Banerjee, I.H. Ali, M.I. Khan and I.-M. Chung, *Constr. Build. Mater.*, **233**, 117320 (2020); https://doi.org/10.1016/j.conbuildmat.2019.117320
5. D.K. Verma, A. Al Fantazi, C. Verma, F. Khan, A. Asatkar, C.M. Hussain and E.E. Ebenso, *J. Mol. Liq.*, **314**, 113651 (2020); https://doi.org/10.1016/j.molliq.2020.113651
6. E.K. Ardakani, E. Kowsari and A. Ehsani, *J. Colloids Surf.*, **586**, 124195 (2020); https://doi.org/10.1016/j.colsurfa.2019.124195
7. A. Thomas, M. Prajila, K.M. Shainy and A. Joseph, *J. Mol. Liq.*, **312**, 113369 (2020); https://doi.org/10.1016/j.molliq.2020.113369
8. J. Narenkumar, P. Parthipan, U.R.N. Ayyakkannu, B.K.M. Giovanni and A. Rajasekar, *J. Biotechnol.*, **7**, 133 (2020); https://doi.org10.1007/s13205-017-0783-9
9. M. Ouakki, M. Galai, S. Rbaa, A.S. Abousalem, B. Lakhrissi, M.E. Touhami and M. Cherkaoui, *J. Mol. Liq.*, **319**, 114063 (2020); https://doi.org/10.1016/j.molliq.2020.114063
10. A. Dehghani, G. Bahlakeh, B. Ramezanzadeh and M. Ramezanzadeh, *J. Mol. Liq.*, **279**, 603 (2019); https://doi.org/10.1016/j.molliq.2019.02.010
11. J. Vicente, F. Calderón, A. Santos, D. Marquina and S. Benito, *Int. J. Mol. Sci.*, **22**, 1196 (2021); https://doi.org/10.3390/ijms22031196
12. C. Verma, E.E. Ebenso, M.A. Quraishi and C.M. Hussain, *J. Mater. Adv.*, **2**, 3806 (2021); https://doi.org/10.1039/D0MA00681E
13. P. Parthipan, P. Elumalai, J. Narenkumar, L.L. Machuca, K. Murugan, O.P. Karthikeyan and A. Rajasekar, *Int. Biodeterior. Biodegrad.*, **132**, 66 (2018); https://doi.org/10.1016/j.ibiod.2018.05.005
14. T. Sathiyapriya, G. Rathika and M. Dhandapani, *J. Adhes. Sci. Technol.*, **33**, 2443 (2019); https://doi.org/10.1080/01694243.2019.1645261
15. A.K. Singh and M.A. Quraishi, *Int. J. Electrochem. Sci.*, **7**, 3222 (2012).
16. M. Solomon and S.A. Umoren, *J. Environ. Chem. Eng.*, **3**, 1812 (2015); https://doi.org/10.1016/j.jece.2015.05.018
17. K.R. Ansari, D.S. Chauhan, M.A. Quraishi, M.A.J. Mazumder and A. Singh, *Int. J. Biol. Macromol.*, **144**, 305 (2020); https://doi.org/10.1016/j.ijbiomac.2019.12.106
18. M. Kashmitha Muthamma, Preethi KumariM.M.Lavanya,M.,Suma and A.Rao, *J. Bio- and Tribo.*, **7**, 10 (2021); https://doi.org/10.1007/s40735-020-00439-7
19. A. Al-Amiery, T.A. Salman, K.F. Alazawi, L.M. Shaker, A.A.H. Kadhum and M.S. Takriff, *Int. J. Low-Carbon Technol.*, **15**, 202 (2020); https://doi.org/10.1093/ijlct/ctz074
20. M. Hanoon, A. Resen, L. Shaker, A. Kadhum and A. Al-Amiery, *Biointerface Res. Appl. Chem.*, **11**, 9735 (2021); https://doi.org/10.33263/BRIAC112.97359743
21. M.V. Fiori-Bimbi, P.E. Alvarez, H. Vaca and C.A. Gervasi, *Corros. Sci.*, **92**, 192 (2015); https://doi.org/10.1016/j.corsci.2014.12.002
22. G. Sigircik, T. Tüken and M. Erbil, *Corros. Sci.*, **102**, 437 (2016); https://doi.org/10.1016/j.corsci.2015.10.036
23. P.R. Ammal, M. Prajila and A. Joseph, *Egypt. J. Pet.*, **27**, 823 (2018); https://doi.org/10.1016/j.ejpe.2017.12.004
24. Z. Tao, S. Zhang, W. Li and B. Hou, *Corros. Sci.*, **51**, 2588 (2009); https://doi.org/10.1016/j.corsci.2009.06.042
25. M. Yadav, L. Gope, N. Kumari and P. Yadav, *J. Mol. Liq.*, **216**, 78 (2016); https://doi.org/10.1016/j.molliq.2015.12.106
26. A. Dutta, S.K. Saha, P. Banerjee and D. Sukul, *Corros. Sci.*, **98**, 541 (2015); https://doi.org/10.1016/j.corsci.2015.05.065
27. A. Popova, M. Christov and A. Vasilev, *Corros. Sci.*, **94**, 70 (2015); https://doi.org/10.1016/j.corsci.2015.01.039
28. M. Yadav, R. Sinha, S. Kumar, I. Bahadur and E.E. Ebenso, *J. Mol. Liq.*, **208**, 322 (2015); https://doi.org/10.1016/j.molliq.2015.05.005
29. E.S. Meresht, T.S. Farahani and J. Neshati, *Eng. Fail. Anal.*, **18**, 963 (2011); https://doi.org/10.1016/j.engfailanal.2010.11.014
30. E.S. Meresht, T.S. Farahani and J. Neshati, *Corros. Sci.*, **54**, 36 (2012); https://doi.org/10.1016/j.corsci.2011.08.052
31. A. Madhankumar and N. Rajendran, *Synth. Met.*, **162**, 176 (2012); https://doi.org/10.1016/j.synthmet.2011.11.028
32. J. Saranya, P. Sounthari, K. Parameswari and S. Chitra, *Measurement*, **77**, 175 (2016); https://doi.org/10.1016/j.measurement.2015.09.008
33. B. Xu, Y. Ji, X. Zhang, X. Jin, W. Yang and Y. Chen, *J. Taiwan Inst. Chem. Eng.*, **59**, 526 (2016); https://doi.org/10.1016/j.jtice.2015.08.020
34. S.J. Alaneme, O. Olusegun and O.T. Adelowo, *Alex. Eng. J.*, **55**, 673 (2016); https://doi.org/10.1016/j.aej.2015.10.009
35. A. Stoyanova, G. Petkova and S.D. Peyerimhoff, *Chem. Phys.*, **279**, 1 (2002); https://doi.org/10.1016/S0301-0104(02)00408-1
36. N.O. Obi-Egbedi, I.B. Obot and M.I. El-Khaiary, *J. Mol. Struct.*, **1002**, 86 (2011); https://doi.org/10.1016/j.molstruc.2011.07.003

37. H.M. Abd El-Lateef, V.M. Abbasov, L.I. Aliyeva, E.E. Qasimov and I.T. Ismayilov, *Mater. Chem. Phys.*, **142**, 502 (2013); https://doi.org/10.1016/j.matchemphys.2013.07.044
38. P. Mourya, P. Singh, R.B. Rastogi and M.M. Singh, *Appl. Surf. Sci.*, **380**, 141 (2016); https://doi.org/10.1016/j.apsusc.2016.01.263
39. D. Zhang, Y. Tang, S. Qi, D. Dong, H. Cang and G. Lu, *Corros. Sci.*, **102**, 517 (2016); https://doi.org/10.1016/j.corsci.2015.10.002
40. K. Krishnaveni and J. Ravichandran, *J. Electroanal. Chem.*, **10**, 1016 (2014); https://doi.org/10.1016/j.jelechem.2014.09.032
41. D.K. Singh, S. Kumar, G. Udayabhanu and R.P. John, *J. Mol. Liq.*, **216**, 738 (2016); https://doi.org/10.1016/j.molliq.2016.02.012
42. J.E. Del Bene, W.B. Person and K. Szczepaniak, *J. Phys. Chem.*, **99**, 10705 (1995); https://doi.org/10.1021/j100027a005
43. F. El-Taib Heakal, A.S. Fouda and M.S. Radwan, *Mater. Chem. Phys.*, **125**, 26 (2011); https://doi.org/10.1016/j.matchemphys.2010.08.067
44. S.E. Nataraja, T.V. Venkatesha, K. Manjunatha, B. Poojary, M.K. Pavithra and H.C. Tandon, *Corros. Sci.*, **53**, 2651 (2011); https://doi.org/10.1016/j.corsci.2011.05.004
45. I. Danaee, O. Ghasemi, G.R. Rashed, M.R. Avei and M.H. Maddahy, *J. Mol. Struct.*, **1035**, 247 (2013); https://doi.org/10.1016/j.molstruc.2012.11.013
46. S.-H. Yoo, Y.-W. Kim, K. Chung, N.-K. Kim and J.-S. Kim, *Ind. Eng. Chem. Res.*, **52**, 10880 (2013); https://doi.org/10.1021/ie303092j
47. F.K. Ekuma Ul-Ekanem and H.O. Chukwuemeka-Okorie, *Int. J. Chem. Stud.*, **6**, 2599 (2018).
48. H.N. Deepakumari, H.D. Revanasiddappa and K.N.N. Prasad, *Vietnam J. Chem.*, **57**, 641 (2019); https://doi.org/10.1002/vjch.201900120
49. M.A. Bedair, M.M.B. El-Sabbah, A.S. Fouda and H.M. Elaryian, *Corros. Sci.*, **128**, 54 (2017); https://doi.org/10.1016/j.corsci.2017.09.016
50. A. Dennis Raj, M. Jeeva, M. Shankar, G. Venkatesa Prabhu, M. Vimalan and I. Vetha Potheher, *J. Mol. Struct.*, **1147**, 763 (2017); https://doi.org/10.1016/j.molstruc.2017.06.133
51. T. Zhang, R. Zhou, P. Wang, A. Mai-Prochnow, R. McConchie, W. Li, R. Zhou, E.W. Thompson, K. Ostrikov and P.J. Cullen, *Chem. Eng. J.*, **421**, 127730 (2016); https://doi.org/10.1016/j.cej.2020.127730
52. A.D. Becke, *J. Chem. Phys.*, **98**, 5648 (1993); https://doi.org/10.1063/1.464913
53. C. Lee, W. Yang and R.G. Parr, *Phys. Rev. B*, **37**, 785 (1988); https://doi.org/10.1103/PhysRevB.37.785
54. R. Ditchfield, W.J. Hehre and J.A. Pople, *J. Chem. Phys.*, **54**, 724 (1971); https://doi.org/10.1063/1.1674902
55. I.B. Obot and Z.M. Gasem, *Corros. Sci.*, **83**, 359 (2014); https://doi.org/10.1016/j.corsci.2014.03.008
56. U. Nazir, Z. Akhter, N.K. Janjua, M.A. Asghar, S. Kanwal, T.M. Butt, A. Sani, F. Liaqat, R. Hussain and F.U. Shah, *RSC Adv.*, **10**, 7585 (2020); https://doi.org/10.1039/C9RA10692H
57. N.M. EL Basiony, A. Elgendy, H. Nady, M.A. Migahed and E.G. Zaki, *RSC Adv.*, **9**, 10473 (2019); https://doi.org/10.1039/C9RA00397E
58. A. Al-Amiery, T.A. Salman, K.F. Alazawi, L.M. Shaker, A.A.H. Kadhum and M.S. Takriff, *Int. J. Low Carbon Technol.*, **15**, 202 (2020); https://doi.org/10.1093/ijlct/ctz074